Vibration Suppression of Plates by Optimally Calibrated Piezoelectric Rl Shunt Damping

Toftekær, Johan Frederik; Høgsberg, Jan Becker; Benjeddou, Ayech; Krenk, Steen

Published in:
Proceedings of the 8th ECCOMAS Thematic Conference on Smart Structures and Materials

Publication date:
2017

Document Version
Publisher's PDF, also known as Version of record

VIBRATION SUPPRESSION OF PLATES BY OPTIMALLY CALIBRATED PIEZOELECTRIC RL SHUNT DAMPING

JOHAN TOFTEKÆR*, JAN HØGSBERG*, AYECH BENJEDDOU†+ AND STEEN KRENK*

*Department of Mechanical Engineering
Technical University of Denmark
Nils Koppels All, Building 404, DK-2800 Kgs. Lyngby, Denmark
e-mail: jotof@mek.dtu.dk, sk@mek.dtu.dk, jhg@mek.dtu.dk/

† Sorbonne Universités, Université de Technologie de Compiègne, CNRS, UMR 7337 ROBERVAL
Centre de Recherche Royallieu, CS 60319, 60203 Compiègne CEDEX, France
e-mail: ayech.benjeddou@utc.fr
+SUPMECA, 3 Rue Fernand Hainaut, 93407 Saint Ouen CEDEX, France
e-mail: benjeddou@supmeca.fr

Key words: RL Shunts, Piezoelectric damping, Structural dynamics, Resonant calibration

Abstract. A calibration procedure for suppression of plate vibrations by means of piezoelectric RL shunt damping is developed, in which the spill-over from non-resonant vibration modes is included by a quasi-dynamic modal correction, taking both flexibility and inertia effects from the residual modes into account. The procedure includes the 2D behaviour of a shunted piezoelectric patch, represented in a finite element model with Kirchhoff plate kinematics. The calibration based on the plate model is compared to previous results for beams, illustrating the 2D effect of the patch and the influence from transverse contraction by the Poisson's ratio. Finally, the ability to reproduce the desired level of attainable damping for a plate structure is demonstrated.

1 INTRODUCTION

The paper concerns suppression of plate vibrations by means of resonant piezoelectric shunt damping. Piezoelectric patches with orthotropic material properties attached locally on a plate are beneficial due to their fairly large force-to-deflection ratio, [1]. Hereby, mechanical energy is effectively converted into electrical energy, which can be dissipated in supplemental resonant shunts.

Piezoelectric vibration damping by a resonant inductive-resistive (RL) shunt was originally suggested by Forward [2] and subsequently developed by Hagood and von Flotow [3], who proposed two calibration procedures based on minimization of response amplitudes and maximization of the damping characteristics, respectively. A corresponding calibration procedure for the parallel RL shunt was subsequently proposed by Wu [4], arguing that the series shunt

would be inappropriate for a large resistance. The series and parallel configurations have been compared by Park and Inman [5], revealing a larger attainable energy dissipation using the parallel configuration, while a summary of the calibration procedures is provided by Caruso [6]. Several alternative procedures for calibration of RL shunts have since been proposed, for instance based on the H_∞-norm of the response amplitude [7]. Recently a calibration procedure based on simultaneous conditions on the dynamic amplification of the structural motion and the relative voltage amplitude of the shunt circuit has been proposed by Høgsberg and Krenk [8], using principles originally developed for the tuned mass damper by Krenk [9]. The procedure has since been extended to include the effect from the non-resonant modes of the structure, initially by a quasi-static correction [10] and subsequently by a quasi-dynamic flexibility and inertia correction [11, 12]. The performance of piezoelectric shunt damping relies on a precise calibration of the shunt frequency, in particular for transducers or patches located indirectly with respect to the deformation pattern of the targeted mode. Thus, the ability to account for the energy spill-over from the non-resonant modes is an important aspect in the calibration of shunt damping of flexible plate structures, with multiple and closely spaced modes.

In the present paper, the calibration procedure described in [12] and illustrated for simple one-dimensional piezoelectric strips on beams is applied to optimal calibration of RL-shunted piezoelectric patches for vibration suppression of plates. Only the parallel RL shunt is considered, while the results may be readily transferred to the corresponding series version. The plate displacements are approximated by a developed finite element model with Kirchhoff plate kinematics, while the piezoelectric patch displacements are considered mainly in-plane with a coupling to the rotations of the plate element. A thorough review of piezoelectric finite elements is provided By Benjeddou [13]. The ability to reproduce the desired level of attainable damping by an optimally calibrated piezoelectric shunt system is demonstrated for beam-like and plate structures. For the beam example, the results obtained with the present plate model are compared to previous results for beams, investigating the contributions from non-resonant modes and the influence of in-plane contraction from the Poisson's ratio effect.

2 MECHANICAL SYSTEM

The dynamics of the considered plate structure is represented by a finite element model based on a Kirchhoff plate element, while a bonded piezoelectric patch acts as external forces at the nodes of attachment. The equation of motion of adaptive the structure can be written as

$$\mathbf{M}\ddot{\mathbf{u}}(t) + \mathbf{K}_0\mathbf{u}(t) + \mathbf{W}\mathbf{f}(t) = \mathbf{f}_e(t) \tag{1}$$

with host structure mass and stiffness matrices $\mathbf{M}$, $\mathbf{K}_0$, patch connectivity matrix $\mathbf{W}$ and force vector $\mathbf{f}(t)$ and external load vector $\mathbf{f}_e(t)$. The degrees of freedom of the structural plate model are contained in the vector $\mathbf{u}(t)$, while structural damping is omitted in the present analysis.

2.1 Structural plate

The plate model is based on Kirchhoff the plate pure bending theory and is discretised by four-node rectangular finite elements. Thus, coupling with an assumed rectangular piezoelectric patch is straightforward. Element-wise Hermitian cubic interpolation is obtained by choosing suitable shape functions for three nodal degrees of freedom (dofs), represented by the lateral

displacement w, and the rotations ϕ_x and ϕ_y about the x- and y-axis, contained in the vector

$$\mathbf{u} = \begin{bmatrix} w_1 & \phi_{x1} & \phi_{y1} & w_2 & \phi_{x2} & \phi_{y2} & \cdots & w_n & \phi_{xn} & \phi_{yn} \end{bmatrix}^T \tag{2}$$

where n is the total node number. The chosen interpolation order must secure C^1 continuity between the elements, associated with second derivatives in the strain definitions. Based on the strains definitions and a weak form representation of the governing equations of motion, the mass matrix $\mathbf{M}$ and stiffness matrix $\mathbf{K}_0$ are obtained for the discretized plate structure.

2.2 Piezoelectric patch

The piezoelectric patch is considered as thin, whereby a simple plane stress assumption is valid, in which transverse stresses are omitted. Further, the electric field is homogeneous through the patch thickness, as the electrodes are evenly distributed on the upper and lower in-plane surfaces. Hereby, the electromechanical coupling between mechanical stresses and strains in an in-plane isotropic patch is governed by the piezoelectric constant e^*, contained in the vector

$$\mathbf{e}_3 = e^*\mathbf{b}, \quad \mathbf{b} = \begin{bmatrix} 1 & 1 & 0 \end{bmatrix}^T \tag{3}$$

The coupled constitutive equations for a 2D plane stress piezoelectric patch can be written as

$$\begin{bmatrix} \boldsymbol{\sigma}_p \\ D_3 \end{bmatrix} = \begin{bmatrix} \mathbf{D}_p & -\mathbf{e}_3 \\ \mathbf{e}_3^T & \varepsilon_{33}^* \end{bmatrix} \begin{bmatrix} \boldsymbol{\varepsilon}_p \\ E_3 \end{bmatrix}, \quad \mathbf{D}_p = \frac{E}{1-\nu^2} \begin{bmatrix} 1 & \nu & 0 \\ \nu & 1 & 0 \\ 0 & 0 & (1-\nu)/2 \end{bmatrix} \tag{4}$$

Here D_3 is the electric displacement, ε_{33}^* is the (blocked) dielectric constant in plane stress, $\boldsymbol{\sigma}_p$ and $\boldsymbol{\varepsilon}_p$ contain the three plane stresses and strains, ν is Poisson's ratio and E is the elastic modulus. The in-plane patch deformations neglect contributions from bending, whereby they can be discretized by four-node rectangular element with two nodal dofs, represented by the in-plane displacements u and v. Thus, the displacement vector for the patch can be arranged as

$$\mathbf{u}_p = \begin{bmatrix} u_1 & v_1 & u_2 & v_2 & u_3 & v_3 & u_4 & v_4 \end{bmatrix} \tag{5}$$

The strains in the patch are now obtained by the first derivatives of the linearly interpolated in-plane displacements. By suitable shape functions N_i in the strain interpolation matrix $\mathbf{B}_p$, the strains can be determined from the nodal displacements as

$$\boldsymbol{\varepsilon}_p = \begin{bmatrix} \varepsilon_{11} \\ \varepsilon_{22} \\ 2\varepsilon_{12} \end{bmatrix} = \mathbf{B}_p\mathbf{u}_p, \quad \mathbf{B}_p = \begin{bmatrix} \partial u/\partial x \\ \partial v/\partial y \\ \partial u/\partial y + \partial v/\partial x \end{bmatrix} \begin{bmatrix} N_1 & 0 & \cdots & N_4 & 0 \\ 0 & N_1 & \cdots & 0 & N_4 \end{bmatrix} \tag{6}$$

The finite element (FE) formulation is now obtained by the so-called weak form of the system of equations in (4), obtained by pre-multiplication with a test function $[\delta\mathbf{u}_p^T \ \delta V]$, followed by integration across the patch area A_p. This weak form equation can be written as

$$\int_{A_p} \begin{bmatrix} \delta\mathbf{u}_p^T & \delta V \end{bmatrix} \begin{bmatrix} \mathbf{B}_p^T\mathbf{D}_p\mathbf{B}_p & \mathbf{B}_p^T\mathbf{e}_3/t_p \\ -\mathbf{e}_3^T\mathbf{B}_p/t_p & \varepsilon_{33}^*/t_p^2 \end{bmatrix} \begin{bmatrix} \mathbf{u}_p \\ V \end{bmatrix} dA_p = \int_{A_p} \begin{bmatrix} \delta\mathbf{u}_p^T & \delta V \end{bmatrix} \begin{bmatrix} \mathbf{B}_p^T\boldsymbol{\sigma}_p \\ -D_3/t_p \end{bmatrix} dA_p \tag{7}$$

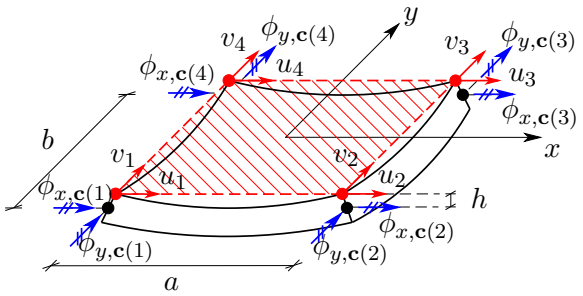

Figure 1: Connectivity between plate element and piezoelectric disk element

in which the electric field E_3 has been replaced by the voltage $V = -E_3 t_p$ across the electrodes. When evaluating the integral, the two coupled constitutive equations for the piezoelectric patch are obtained as

$$\mathbf{f} = \int_{A_p} \mathbf{B}_p^T \boldsymbol{\sigma} A_p = \mathbf{k}_p \mathbf{u}_p + \mathbf{T}_p^T \mathbf{b} k V \quad , \quad q = -D_3 A_p / t_p = -\theta \mathbf{b}^T \mathbf{T}_p \mathbf{u}_p + CV \tag{8}$$

where q is the charge. In these governing equations the piezoelectric element stiffness matrix $\mathbf{k}_p$, the integrated strain interpolation matrix $\mathbf{T}_p$, the electromechanical coupling coefficient θ and the capacitance C for blocked patch boundaries ($\mathbf{u}_p = \mathbf{0}$) have been introduced as

$$\mathbf{k}_p = \int_{A_p} \mathbf{B}_p^T \mathbf{D}_p \mathbf{B}_p dA_p, \quad \mathbf{T}_p = \int_{A_p} \mathbf{B}_p dA_p, \quad \theta = e^*/t_p, \quad C = A_p \varepsilon_{33}^*/t_p^2 \tag{9}$$

In (8a) the force vector $\mathbf{f}$ depends on both the patch stiffness $\mathbf{k}_p$ and the electromechanical coupling. The latter is in the following dynamic analysis represented by the piezoelectric force

$$f_p = \theta V \tag{10}$$

which is proportional to the voltage V across the electrodes.

2.3 Coupled piezo-structure system

The piezoelectric patch is now coupled with the structural plate model, as illustrated in Fig. 1, where $\mathbf{c}$ contains the particular nodes of the structural plate model that are connected to the piezoelectric patch. The distance from the midplane of the plate to the midplane of the patch is defined by h (positive upwards), whereby the rotations ϕ_x and ϕ_y of the plate generate in-plane displacements v and u in the patch, as given by the kinematic relation

$$u_i = h\phi_{y,\mathbf{c}(i)}, \quad v_i = -h\phi_{x,\mathbf{c}(i)}, \quad i = 1,2,3,4 \tag{11}$$

where the minus follows from the kinematics associated with a Kirchhoff plate. The relation between the in-plane patch displacements and the rotations of the plate in $\mathbf{u}$ are defined as

$$\mathbf{u}_p = \mathbf{W}^T \mathbf{u}, \quad \mathbf{W}^T = \begin{bmatrix} 0 & \cdots & 0 & 0 & 0 & h & \cdots & & & 0 & \cdots & 0 \\ 0 & \cdots & 0 & 0 & -h & 0 & \cdots & & & 0 & \cdots & 0 \\ \vdots & \ddots & \vdots & & & & \ddots & & & \vdots & \ddots & 0 \\ 0 & \cdots & 0 & & & & \cdots & 0 & 0 & h & 0 & \cdots & 0 \\ 0 & \cdots & 0 & & & & \cdots & 0 & -h & 0 & 0 & \cdots & 0 \end{bmatrix} \tag{12}$$

Node $\mathbf{c}(1)$ Node $\mathbf{c}(4)$

where the 12 non-zero columns in the connectivity matrix $\mathbf{W}$ uniquely establish the coupling in (11) with the structural plate model at the location of the patch. When substituting the force vector in (8a), the equation of motion (1) for the coupled piezo-plate system can be written as

$$\mathbf{M}\ddot{\mathbf{u}}(t) + \underbrace{(\mathbf{K}_0 + \mathbf{W}\mathbf{k}_p\mathbf{W}^T)}_{\mathbf{K}}\mathbf{u}(t) + \underbrace{\mathbf{W}\mathbf{T}_p^T\mathbf{b}}_{\mathbf{w}} f_p(t) = \mathbf{f}_e(t) \tag{13}$$

where the piezoelectric patch introduces a stiffness contribution $\mathbf{k}_p$ to the mechanical system, while the voltage dependent force f_p is determined by the shunt circuit impedance.

2.4 Shunt damping

The electromechanical properties of the piezoelectric patch depend on the apparent voltage V in the transverse 3-direction, governed by the shunt impedance $Z(\omega)$ via the relation

$$V = -i\omega Z(\omega) Q. \tag{14}$$

in the frequency domain, assuming a temporal dependence represented by the complex exponential factor $\exp(i\omega t)$ with assumed angular frequency ω. The charge in (8b) is now eliminated through this impedance relation, and the derived expression for the voltage is subsequently substituted into (10) to obtain the following flexibility relation,

$$u_p = \mathbf{w}^T\mathbf{u} = \left(\frac{C}{\theta^2} + \frac{1}{i\omega\theta^2 Z(\omega)}\right) f_p, \tag{15}$$

For the parallel RL-shunt circuit, the inverse of the impedance function is

$$\frac{1}{Z(\omega)} = \frac{1}{R} + \frac{1}{i\omega L} \tag{16}$$

and substitution of $Z(\omega)$ into (15) gives

$$u_p = \left(\frac{C}{\theta^2} + \frac{1}{i\omega R\theta^2} - \frac{1}{\omega^2 L\theta^2}\right) f_p \tag{17}$$

which represents a mechanical model of a spring (θ^2/C), damper ($R\theta^2$) and inerter ($L\theta^2$) placed in series. The coupled system equations are represented by (13) and (17) with $\mathbf{w} = \mathbf{W}\mathbf{T}_p^T\mathbf{b}$.

3 MODAL CALIBRATION PROCEDURE

The components of the RL shunt are calibrated with respect to a targeted vibration mode of the structure. With shorted transducer electrodes ($V = 0$), the homogeneous form of the equations of motion (13) reduces to this eigenvalue problem

$$(\mathbf{K} - \omega_j^2\mathbf{M})\mathbf{u}_j = \mathbf{0} \tag{18}$$

Based on the normalized mode shape $\mathbf{u}_j/(\mathbf{w}^T\mathbf{u}_j)$, the j'th equation of motion (13) becomes

$$(-\omega^2 m_j + k_j)u_j + f_p = f_j \tag{19}$$

where m_j, k_j and f_j are modal mass, stiffness and load, respectively. The resulting patch displacement u_p is now represented by the contribution u_r from the resonant mode ($j = r$) and an additional contribution from the non-resonant vibration modes ($j \neq r$). As shown in [11] the following approximate representation captures the contribution of higher and lower frequency modes around the resonant frequency,

$$u_p = u_r - \left(\frac{1}{k'_r} - \frac{1}{k''_r} \frac{\omega_r^2}{\omega^2} \right) f_p \tag{20}$$

where the contribution from the non-resonant resonant modes is represented by supplemental flexibility and inertia via the two modal coefficients [12]

$$\frac{1}{k'_r} = \mathbf{w}^T \mathbf{K}_r^{-1} \mathbf{K} \mathbf{K}_r^{-1} \mathbf{w} - \frac{1}{k_r} \quad , \quad \frac{1}{k''_r} = \mathbf{w}^T \mathbf{K}_r^{-1} \mathbf{K} \mathbf{K}_r^{-1} \mathbf{w} - \mathbf{w}^T \mathbf{K}_r^{-1} \mathbf{w} \tag{21}$$

using a frequency shifted form of the stiffness matrix

$$\mathbf{K}_r = \mathbf{K} - \omega_r^2 \mathbf{M}_r \quad , \quad \mathbf{M}_r = \mathbf{M} - \frac{(\mathbf{M}\mathbf{u}_r)(\mathbf{M}\mathbf{u}_r)^T}{\mathbf{u}_r^T \mathbf{M} \mathbf{u}_r} \tag{22}$$

in which case the inertia of the resonant modes is removed in the corresponding mass matrix $\mathbf{M}_r$. The resulting patch displacement determined by (17) can now be substituted into (20),

$$u_r = \left(\frac{C}{\theta^2} - \frac{1}{\omega^2 L \theta^2} + \frac{1}{i\omega R \theta^2} + \frac{1}{k'_r} - \frac{1}{k''_r} \frac{\omega_r^2}{\omega^2} \right) f_p \tag{23}$$

It is seen that the flexibility and inertia correction terms can be combined with the capacitance and inductance, respectively. The flexibility relation in (23) is then reduced to

$$u_r = \frac{C_r}{\theta^2} \left(1 - \frac{1}{\omega^2 L_r C_r} + \frac{1}{i\omega R C_r} \right) f_p \tag{24}$$

introducing a modal capacitance C_r and a modal inductance L_r as

$$C_r = (1 + \kappa'_r) C \quad , \quad L_r C_r = L \left(C_r + \frac{1}{\kappa''_r \omega_r L} \right) \tag{25}$$

where the non-dimensional correction coefficients are defined as

$$\kappa'_r = \frac{\theta^2}{k'_r C} \quad , \quad \kappa''_r = \frac{\theta^2}{k''_r C_r} \tag{26}$$

The balanced calibration with equal modal damping used in [12] is now used for the optimal tuning of the shunt inductance L and resistance R, which are obtained by the expressions

$$LC\omega_r^2 = \frac{1}{(1 + \kappa'_r)(1 - \kappa''_r)}, \quad RC\omega_r = \frac{1}{1 + \kappa'_r} \sqrt{\frac{1}{2\kappa_r}} \tag{27}$$

It is seen that the inductance depends both on the flexibility and inertia corrections, while the magnitude of the shunt resistance is only influenced by the flexibility coefficient κ'_r.

4 NUMERICAL EXAMPLES

In the following both a beam and a plate structure with piezoelectric patches are analyzed, demonstrating the influence from non-resonant modes in the calibration of RL-shunts.

4.1 Cantilever beam

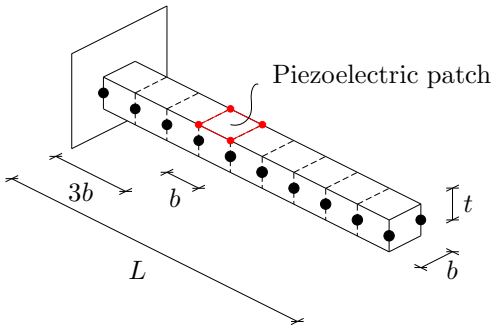

Figure 2: Geometry and discretization of cantilever beam by use of plate elements.

The first example concerns a cantilever beam with a piezoelectric patch shown in Fig. 2, which also indicates the discretisation and dimensions, where the width is given $b = L/10$ and the thickness is determined by $t = b/100$, hence the use of Kirchhoff plate bending theory appears valid. Initially a Poisson's ratio of $\nu = 0$ is considered for both plate and patch, chosen in order to compare with the results for a beam model. Both the thickness and elastic modulus of the patch are assumed to be $t_p = t/4$ and $E_p = E/4$, respectively. The natural frequencies for the beam without the patch (ω_0) and with shorted electrodes (ω_r) are in Table 1 normalized by the analytical value $\omega_a = (1.875)^2\sqrt{EI/(\rho AL^4)}$ for a cantilever. The table also provides the calibrated shunt components, the correction parameters and the attained damping ratios for the beam modeled by plate elements (ζ_r) and for a pure beam model [12]. The final column in the table presents the damping ratio ζ_{rb} for the plate model when using the calibrated parameters from the beam model. The first six mode shapes for the plate model are shown in Fig. 3. However, only results for the five bending modes are presented in Table 1, as the torsional mode (d) in Fig. 3 can not be attenuate by the present patch model.

Table 1: Optimal calibration of the electronic components, for respectively the beam and plate model

Mode	ω_0/ω_a	ω_r/ω_a	$LC\omega_r^2$	$1/(RC\omega_r)$	κ_r'	κ_r''	ζ_r		ζ_{rb}	
1	1.0000	1.0088	0.8771	0.1825	0.1405	0.0003	0.0400	0.0400	–	–
2	6.2671	6.3109	0.8561	0.1877	0.1733	0.0045	0.0400	0.0400	–	–
3	17.5519	17.7617	0.9314	0.1724	0.0772	0.0033	0.0400	0.0400	–	–
4	34.4188	34.4208	–	–	–	–	–	–	–	–
5	56.9859	57.5794	0.9225	0.1777	0.1104	0.0237	0.0401	0.0399	–	–
1	1.0000	1.0088	0.8031	0.1993	0.2457	0.0004	0.0400	0.0400	0.0237	0.0534
2	6.2661	6.3099	0.7754	0.2073	0.2958	0.0048	0.0400	0.0400	0.0216	0.0550
3	17.5313	17.7410	0.8919	0.1800	0.1252	0.0036	0.0400	0.0400	0.0291	0.0489
4	34.2787	34.2814	–	–	–	–	–	–	–	–
5	56.4311	57.0179	0.8880	0.1848	0.1552	0.0251	0.0402	0.0400	0.0313	0.0464

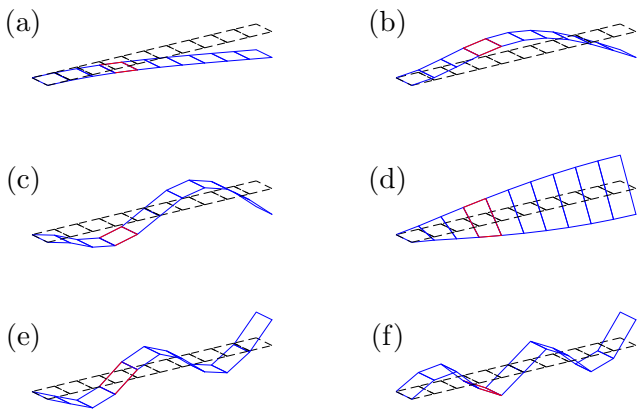

Figure 3: Vibration modes 1-6 ((a)-(f)) for the cantilever beam discretized by plate elements

Good agreement is observed when comparing the natural frequencies for the beam and plate models in Table 1. For each mode the shunt transducer parameters are determined by the balanced calibration formulae in (27) based on a desired damping ratio $\zeta_r^{\rm des}$, which can be predicted by the design expression $\kappa_r = 8(\zeta_r^{\rm des})^2 = 0.0128$, as explained in [12]. The normalized shunt parameters exhibit significant deviations, when comparing the beam and plate models, mainly due to the influence from the non-resonant modes. It is especially observed for the flexibility coefficient κ_r', which in Table 1 is larger for the plate model because of a more substantial contribution from non-resonant modes. The fourth bending mode can not be attenuated, as the patch is located at a nodal point of the vibration form shown in Fig 3(e).

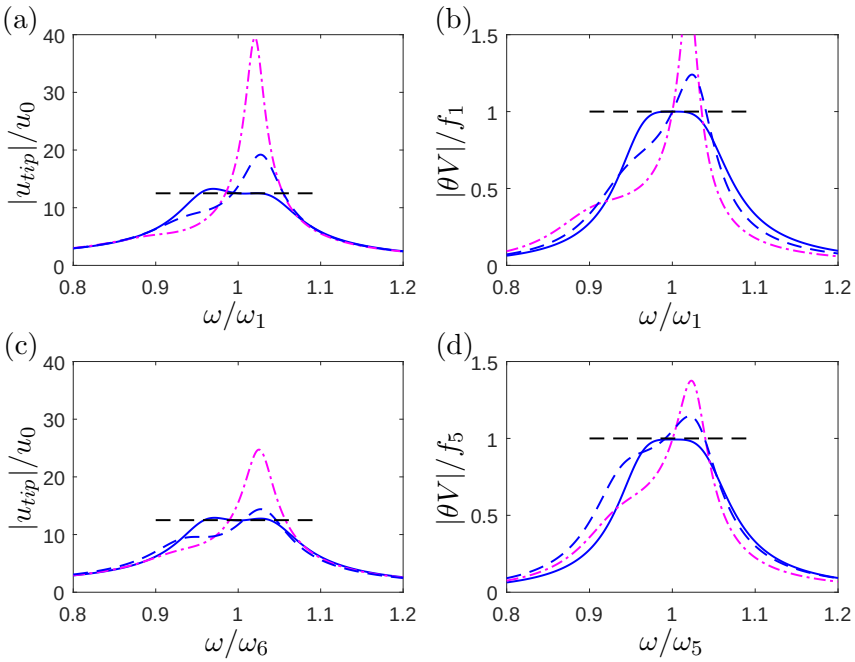

Figure 4: (a,c) Dynamic amplification, and (b,d) Voltage amplitude, calibrated for mode $r = 1, 5$

The dynamic amplification of the tip displacement and the frequency amplitude of the corresponding transducer force f_p is shown on Fig. 4 for bending modes 1 and 5. The (blue) solid curve represents the optimal calibration from the beam and plate models, the (blue) dashed curve represents the beam model calibration used in the plate model, and the (magenta) dashed-dotted curve represents the calibration where the residual mode correction is neglected ($\kappa_r' = 0$ and $\kappa_r'' = 0$). It is seen that the optimally calibrated models recover the desired level of vibration mitigation (horizontal dashed line), while when using the beam model calibration in the plate model a substantial off-tuning is observed, due to the apparent misrepresentation of the spill-over from the non-resonant modes. Furthermore, the calibration without residual mode correction also yields a large increase in vibration amplitude.

The effect of in-plane contraction, which in particular will cause significant contraction of the beam width, is now investigated for a Poisson's ratio of $\nu = 0.3$. The natural frequencies and calibration parameters are presented in Table 2. It is seen that the inclusion of this effect has a significant impact on the calibration results, while the changes in natural frequency are only moderate. The mistuning obtained by neglecting the Poisson's ratio effect is illustrated by the damping ratio $\zeta_{r,\nu=0}$ obtained when using the calibration determined for $\nu = 0$. It shows a considerable reduction in the attainable damping, and a sufficiently accurate model should therefore be used for calibration of piezoelectric shunts, see [14].

Table 2: Optimal shunt calibration for plate model of cantilever beam, with $\nu = 0.3$

Mode	ω_0/ω_a	ω_r/ω_a	$LC\omega_r^2$	$1/(RC\omega_r)$	κ_r'	κ_r''	ζ_r		$\zeta_{r,\nu=0}$	
1	1.0078	1.0169	0.6725	0.2380	0.4875	0.0004	0.0400	0.0400	0.0233	0.0584
2	6.3373	6.3806	0.6194	0.2597	0.6229	0.0052	0.0400	0.0400	0.0243	0.0577
3	17.8812	18.0972	0.8250	0.1947	0.2166	0.0037	0.0400	0.0400	0.0272	0.0537
4	35.4038	35.4101	–	–	–	–	–	–	–	–
5	59.5008	59.7209	0.8344	0.1971	0.2319	0.0272	0.0400	0.0403	0.0187	0.0633

4.2 Plate structure

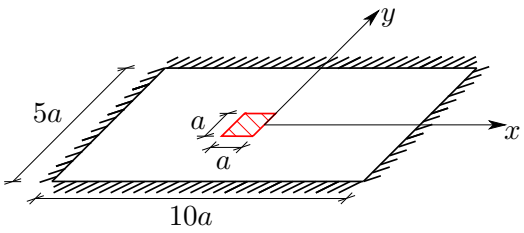

Figure 5: Geometry of simple plate structure with patch centred about the x-axis and right patch edge following the y-axis.

A piezoelectric patch is now coupled to a simple plate structure, see Fig. 5, with the patch placed with a small offset from the center, so that the right patch edge follows the central y-axis. This placement is chosen in order to avoid nodal points for the targeted vibration modes at the center of the plate. The plate thickness is $t = a/100$ and the patch thickness and elastic modulus are defined as in the previous example, while Poisson's ratio for both patch and plate are $\nu = 0.3$,

Table 3: Optimal shunt calibration for plate structure.

Mode	ω_0/ω_a	ω_r/ω_a	$LC\omega_r^2$	$1/(RC\omega_r)$	ζ_r		ζ_r^q		ζ_r^0	
1	0.9919	0.9968	0.9662	0.0829	0.0200	0.0200	0.0197	0.0202	0.0125	0.0268
2	1.5681	1.5688	0.6332	0.1360	0.0200	0.0200	0.0123	0.0255	0.0010	0.0314
3	2.5313	2.5399	0.9581	0.0839	0.0200	0.0200	0.0192	0.0206	0.0112	0.0278
4	3.3747	3.3748	–	–	–	–	–	–	–	–
5*	3.8869	3.8913	–	–	–	–	–	–	–	–
6*	3.8862	3.8924	0.8970	0.0920	0.0200	0.0200	0.0167	0.0224	0.0056	0.0316

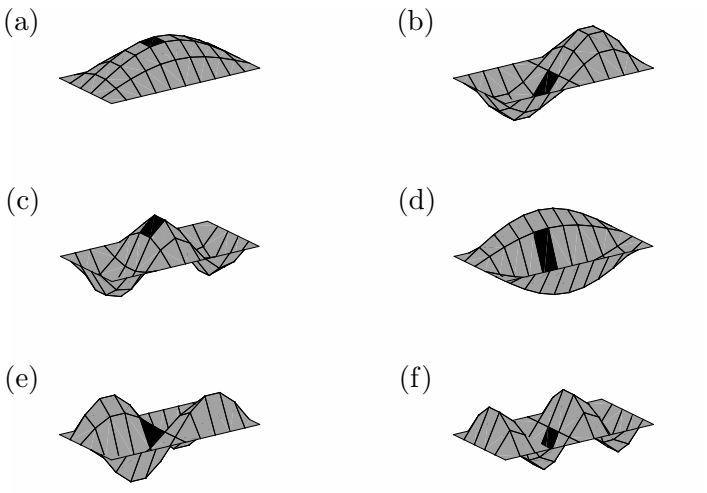

Figure 6: Vibration mode 1-6((a)-(f)) for the rectangular plate with piezoelectric patch

whereas the mass of the patch is neglected. The natural frequencies are again normalized by the analytical solution $\omega_a = \sqrt{D/(\rho t)}\left(\pi^2/(5a)^2 + \pi^2/(10a)^2\right)$ for the first plate vibration mode with bending stiffness $D = \frac{Et^3}{12(1-\nu^2)}$. The piezoelectric shunt is calibrated according to a desired damping ratio $\zeta_{des} = 0.02$, which gives the modal coupling coefficient $\kappa_r = 8(\zeta_r^{\rm des})^2 = 0.0032$. The plate has been discretized by 10×5 Kirchhoff plate elements and the piezoelectric patch is represented by a single element. The first six natural frequencies and corresponding mode shapes are investigated, and the optimal calibration for each mode is presented in Table 3. The mode shapes are shown in Fig. 6, where the black element indicates the patch position. Table 3 also presents the damping ratios ζ_r^q and ζ_r^0, achieved by a quasi-static correction ($\kappa_r'' = 0$) and without correction ($\kappa_r' = 0$ and $\kappa_r'' = 0$), respectively. It is found that when not including the full residual mode correction, with both flexibility and inertia contributions, substantial mistuning might occur. Thus, it is important to consider the spill-over effect from residual modes in the calibration procedure of RL shunts. For mode 4, the patch is located at a nodal point and can therefore not be attenuated. Vibration modes $r = 5$ and 6 have practically identical frequencies, and when attaching the piezoelectric patch they even interchange order. However, it is seen that mode 5 can not be attenuated because the patch is exposed to torsion deformations, thus is in pure shear.

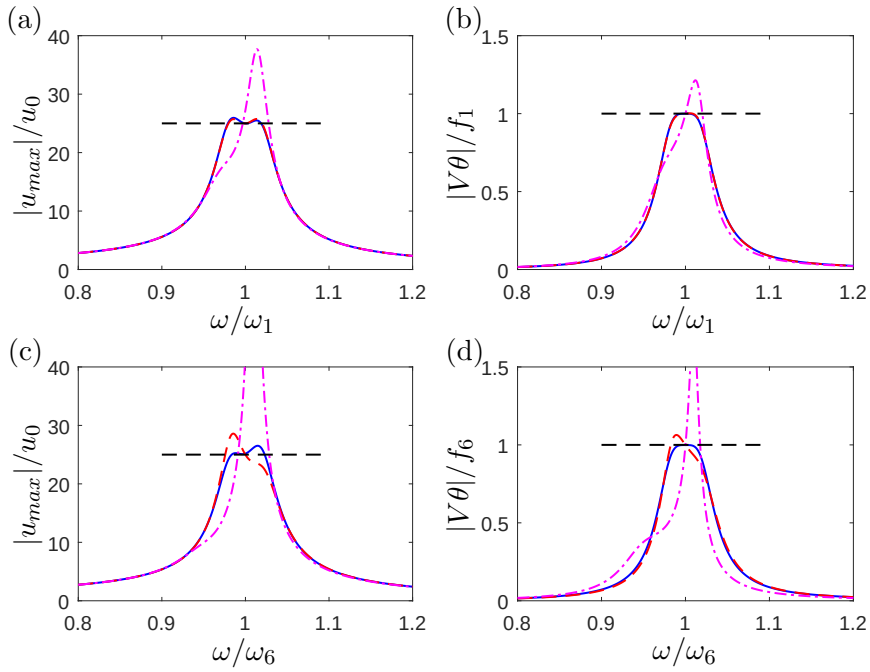

Figure 7: Dynamic amplification (a,c) and force amplitude (b,d) for modes $r = 1$ and 6.

Figure 7 shows the dynamic amplification of the plate structure at the specific position of maximum amplitude and the shunt force f_p for modes $r = 1$ and 6. The solid curve shows the response for the present calibration procedure, the dashed curve shows the case with only quasi-static correction ($\kappa_r'' = 0$), while the dotted-dashed curve shows the structural amplitude in the case without residual mode correction. The black dashed line indicates the desired amplitude level, which is attained by the fully corrected calibration, while substantial amplification is observed when the residual mode correction is not included.

5 CONCLUSIONS

The balanced calibration procedure based on equal modal damping and with compensation for spill-over from residual modes has been successfully implemented for plate structures with an RL shunted piezoelectric patch. The importance of a precise structural model has been shown by comparing results for a cantilever beam, modeled by beam and plate elements, respectively. For the plate model of the cantilever, the 2D behavior of the piezo-plate model captures additional dynamic effects that improve the accuracy of the calibration procedure. Furthermore, the inclusion of in-plane contraction from a non-vanishing Poisson's ratio is important in order to obtain a precise RL shunt calibration. Finally, a finite element scheme and calibration procedure has been investigated for piezoelectric shunt damping of plate structures, based on a desired level of damping in the targeted vibration mode. It has been demonstrated that a consistent correction with respect to the flexibility and inertia contributions from non-resonant modes is important. In future work, the contribution from the bending stiffness of the piezoelectric patch will be

included, improving the model accuracy. Furthermore, a refined mesh of the plate and patch is introduced to achieve full convergence of the natural frequencies, the residual mode corrections coefficients and the calibrated shunt components.

ACKNOWLEDGEMENT

This research has been supported by the Danish Council for Independent Research via the project 'Resonant Piezoelectric Shunt Damping of Structures'.

REFERENCES

[1] Preumont, A., *Vibration Control of Active Structures. An Introduction*, 3rd edition, Springer, Heidelberg, 2011.

[2] R.L. Forward, Electronic damping of vibrations in optical structures, *Applied Optics* (1979) **18**:690–697.

[3] Hagood, N.W., von Flotow, A., Damping of structural vibrations with piezoelectric materials and passive electrical networks, *Journal of Sound and Vibration* (1991) **146**:243-268.

[4] Wu, S.Y., Piezoelectric shunts with a parallel R-L circuit for structural damping and vibration control, *SPIE Proceedings* (1996) **2720**:259-269.

[5] Park, C.H., Inman, D.J. A uniform model for series R-L and parallel R-L shunt circuits and power consumption, *SPIE Proceedings*, (1999) **3668**:797804.

[6] Caruso, G., A critical analysis of electric shunt circuits employed in piezoelectric passive vibration damping, *Smart Materials and Structures*, (2001)**10**:1059-1068.

[7] Soltani, P., Kerschen, G., Tondreau, G., Deraemaeker, A., Piezoelectric vibration damping using resonant shunt circuits: an exact solution, *Smart Materials and Structures*, (2014) **23**:125014 (11pp).

[8] Høgsberg, J., Krenk, S., Balanced calibration of resonant shunt circuits for piezoelectric vibration control, *Journal of Intelligent Material Systems and Structures* (2012) **23**:1937-1948.

[9] Krenk, S. Frequency analysis of the tuned mass damper, *Journal of Applied Mechanics*, (2005) **72**:936-942.

[10] Høgsberg, J., Krenk, S. Balanced calibration of resonant piezoelectric RL shunts with quasi-static background flexibility correction, *Journal of Sound and Vibration* (2015) **341**:16-30.

[11] Krenk, S., Høgsberg, J., Tuned resonant mass or inerter-based absorbers: Unified calibration with quasi-dynamic flexibility and inertia correction, *Proceedings of the Royal Society A-Mathematical, Physical and Engineering Sciences* (2015) **472**:20150718 (23 pp).

[12] Høgsberg, J., Krenk, S., Calibration of piezoelectric RL shunts with explicit residual mode correction, *Journal of Sound and Vibration*, (2017) **386**:65-81

[13] Benjeddou, A., Advances in piezoelectric finite element modeling of adaptive structural elements: a survey, *Computers and Structures*, **76** (2000) 347-363.

[14] Benjeddou, A., Modal effective electromechanical coupling approximate evaluations and simplified analyses: Numerical and experimental assessments, *Acta Mechanica*, **225** (2014) 2721-2742.